Characterization of Scale Factor Nonlinearities in Coriolis Vibratory Gyroscopes

Daryosh Vatanparvar, Mohammad H. Asadian, Sina Askari, and Andrei M. Shkel
MicroSystems Laboratory, Mechanical and Aerospace Engineering, University of California, Irvine, CA, USA
Email: {dvatanpa, asadianm, askaris, and andrei.shkel}@uci.edu

***Abstract*—In this paper, we studied the mechanisms which contribute to Scale Factor (SF) nonlinearity in Coriolis Vibratory Gyroscopes (CVG) operating in the open-loop angular rate mode. Analytical equations were derived to quantify the effects of electro-mechanical nonlinearities, modal coupling, and nonlinear capacitive sensing on SF. Experimental results with a Dual Foucault Pendulum (DFP) gyroscope are presented and compared to simulated data of the predictive model. In our experiments, we demonstrated that by minimizing the electro-mechanical nonlinearities, the SF error is reduced by 27.7% at the angular rate of 1 Hz. We concluded that modal coupling is the major source of SF nonlinearity. We also concluded that nonlinearity in the capacitive sensing has the lowest contribution to SF nonlinearity, at angular rates up to 1 Hz. Finally, we discussed conditions under which a linear SF can be achieved.**

I. Introduction

Open-loop angular rate measurement is a frequently used mode of operation in Coriolis Vibratory Gyroscopes (CVG). A superior noise performance and a lower complexity in implementation, as compared to the closed-loop rate mode of operation, are among the major advantages of the open-loop operation, [1]. However, a low Band Width (BW) and the Scale Factor (SF) nonlinearity are among limitations of the open-loop operation. In this paper, we investigated the mechanisms which influence the linearity of SF and discussed the conditions under which the linearity of SF can be improved.

In the open-loop rate mode of operation, the amplitude and phase of vibration along the drive axis is contained at a specified value and the vibration amplitude along the sense axis is used to measure the angular rate input. The amplitude of the Coriolis signal along the sense axis is dependent on the frequency split between the operational modes and the quality factor in the sense mode. In a relatively low Q-factor CVG (around a few tens of thousands), with a high frequency split relative to the bandwidth of the sense mode, the vibration amplitude along the sense axis is orders of magnitude smaller than the drive axis. Under such conditions, nonlinearities due CVGs' dynamics, parallel plate capacitive sensing, and coupling forces along the drive axis can be neglected. However, to achieve a higher sensitivity and realize the navigational grade Micro-Electro Mechanical (MEM) CVGs, a high Q-factor (hundreds of thousands) and nearly mode-matched conditions are necessary, [2, 3]. Under such conditions, the SF linearity is adversely affected by a large vibration amplitude along the sense axis and the SF errors are introduced. In this paper, we studied mechanisms such as electro-mechanical nonlinearities, modal coupling, and nonlinear capacitive sensing as possible sources of SF nonlinearity in a nearly isotropic high-Q gyroscope. Modeling results are presented to understand the contribution of each of these mechanisms to the SF nonlinearity. A Dual Foucault Pendulum (DFP) is an example of a high-Q gyroscope with a symmetric design, Fig. 1. For this device, the SF characterization was performed and the behavior was explained by predictive models.

This material is based on work supported by the Defense Advanced Research Projects Agency (DARPA) and U.S. Navy under Contract No. N66001-16-1-4021.

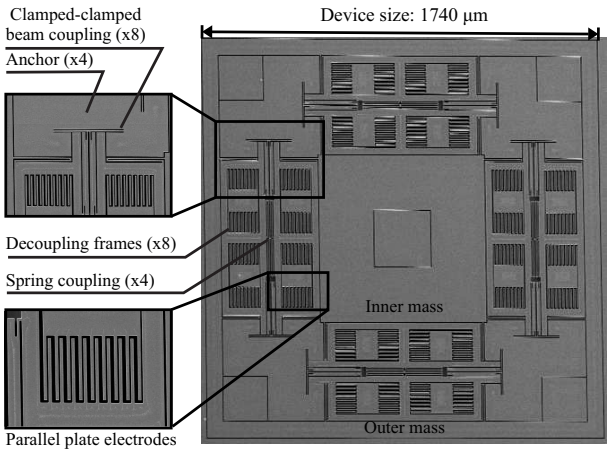

Fig. 1. Schematics of the DFP with parallel plate electrodes for actuation, tuning, and detection. $Q_x = 1.12M$, $Q_y = 1.15M$, $\omega_x = 15.03\ kHz$, and $\omega_y = 15.14\ kHz$ are characteristics of the DFP at room temperature, [3, 4].

II. Nonlinear Dynamics of CVGs

Nonlinear dynamics is often a neglected characteristic of MEMS gyroscopes. In presence of electro-mechanical nonlinearities, variation in the amplitude of vibration along each principal axis of elasticity affects the resonant frequency of that axis. The effect of nonlinear dynamics on SF is modeled by considering a nonlinear equation of motion along the sense axis

$$\ddot{y} + 2\mu_{0y}\dot{y} + \omega_{ny}^2 y + \beta_y y^3 = 2\dot{x}\Omega + f_e, \qquad (1)$$

where μ_{0y}, ω_{ny}^2 and β_y are the linear damping coefficient, linear stiffness, and the geometric Duffing nonlinearity along the sense axis, respectively. It should be noted that for simplicity, the quadrature coupling and the coupling forces along the drive axis are neglected in this analysis and will be discussed in the next section.

978-1-5386-7828-2/19/$31.00 ©2019 IEEE

The velocity along the drive axis is defined as

$$\dot{x} = X_a \omega_{0x} cos(\omega_{0x} t) \tag{2}$$

By assuming a non-rotating device ($\Omega = 0$), the ring down response can be used to estimate the linear and nonlinear parameters in Eqn. (1). The electrostatic force in the parallel plate drive architecture is calculated as

$$f_e = \frac{1}{2m} \frac{C_0 g}{(g-y)^2} V^2, \tag{3}$$

where m, C_0, g and V are the mass, nominal capacitance, gap size in the capacitive actuator, and the actuation voltage, respectively. The nonlinear force can be expanded by writing the Taylor series of the forcing function about system's zero deflection point ($y = 0$). In the case of a push-pull drive architecture, the Taylor expansion can be written as

$$f_e = \sum_{j=1}^{2n+1} k_j y^j V^2 \tag{4}$$

In Eqn. (4), the even order terms are canceled out due to symmetry of the exerted forces. The coefficient (k_j) is calculated as

$$k_j = \frac{0.5 C_0}{(j+1) m g^{j+1}}, \tag{5}$$

The equation of motion describing the sense mode with only the biasing voltages applied ($V = V_{dc}$) is shown below, considering nonlinearities up to the 3rd order,

$$\ddot{y} + 2\mu_{0y}\dot{y} + \omega_{0y}^2 y + \beta_y' y^3 = 0 \tag{6}$$

The modified coefficients, relative to Eqn. (1), capture the frequency shift and induced 3rd order nonlinearity due to electrostatic forces and are defined as

$$\omega_{0y}^2 = \omega_{ny}^2 - k_1 V_{dc}^2, \quad \beta_y' = \beta_y - k_3 V_{dc}^2 \tag{7}$$

In [5], it is demonstrated that assuming a slow-varying amplitude and phase during the ring down, a pure harmonic oscillation form can be used to describe the response with time-varying amplitude and phase,

$$y(t) = a(t) sin(\omega_{0y} t + \phi(t)) \tag{8}$$

The amplitude of vibration and resonant frequency in the ring down response is calculated as

$$a(t) = a_0 e^{-\mu_{0y} t}, \quad \omega_y(t) = \omega_{0y} + (\frac{3\beta_y'}{8\omega_{0y}}) a(t)^2, \tag{9}$$

where a_0 is the initial vibration amplitude, [6]. Using Eqn. (9) and applying the nonlinear least square method, the ring down response was used to estimate the linear and nonlinear system parameters of the sense mode described by Eqn. (6), Fig. 2. The experiment was repeated for four different tuning voltages to decouple the contribution of electrostatic forces to the 3rd order nonlinearity, using Eqn. (7).

As shown in Eqn. (10), the SF is estimated through solving the equation for the amplitude of the steady-state response

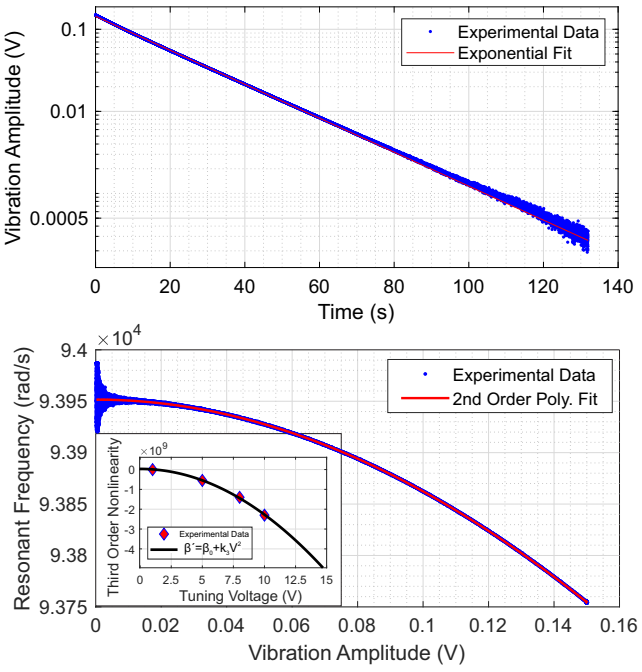

Fig. 2. The ring down response along the sense axis with an initial amplitude of 150mV is shown, illustrating the variations of the resonant frequency during the ring down. The experimental data and equations in (9) were used to extract parameters of the equation of motion for a tuning voltage of (10V).

TABLE I
EXTRACTED PARAMETERS USING MULTIPLE RING DOWNS

a_0 (mV)	μ_{0y} $(1/s)$	ω_{0y} (rad/s)	β_y	k_3
150	0.048	9.39e4	2e7	2.3e7

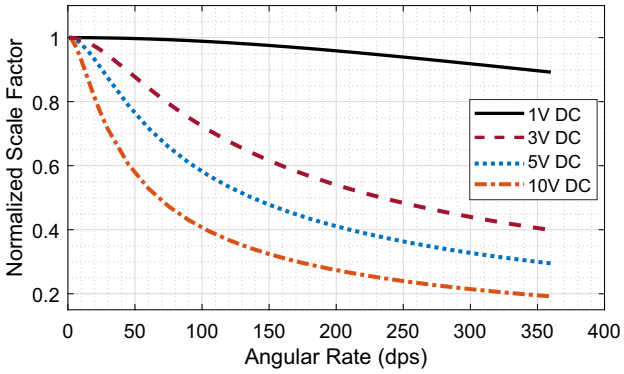

Fig. 3. Shown is the simulated SF, assuming a nonlinear equation of motion along the sense axis. The parameters used for modeling are: $X_a = 0.1$, $\omega_x = 15\ kHz$, $\Delta f = 0.5\ Hz$, quality factor of 1M, and tuning voltages varying from 1V to 10V.

in a nonlinear mass-spring-damper with parameters shown in Table I. The modeling was repeated for different DC tuning voltages applied along the sense axis, Fig. 3.

$$Y_c = \frac{2 X_a \omega_{0x} \Omega}{\sqrt{((\omega_{0y} + (\frac{3\beta_y'}{8\omega_{0y}}) Y_c^2)^2 - \omega_{0x}^2)^2 + (2\omega_{0x}\mu_{0y})^2}} \tag{10}$$

III. Modal Coupling in CVG

In a CVG, the rotation induced Coriolis forces and stiffness imbalances due to the fabrication imperfections couple the drive and sense modes, [7]. The equation of motion in the matrix form is represented as

$$\ddot{q} + Z\dot{q} + Kq = F(t), \tag{11}$$

where the column vector q is the position of the proof mass along the x and y axes. In Eqn. (11), Z and K matrices are:

$$Z = \begin{bmatrix} C_x & -2\alpha\Omega \\ 2\alpha\Omega & C_y \end{bmatrix}, K = \begin{bmatrix} \omega_x^2 & \omega_{xy}^2 \\ \omega_{xy}^2 & \omega_y^2 \end{bmatrix} \tag{12}$$

where C_x, ω_x, C_y, and ω_y are the damping and stiffness coefficients of the drive and sense modes, respectively. The coupling due to the Coriolis force and stiffness imbalances is represented through off-diagonal elements of the Z and K matrices. In Eqn. (12), α, Ω and ω_{xy} are the angular gain, angular rate, and stiffness coupling. The K matrix can be calculated using the resonant frequencies ω_{0x}, ω_{0y} and the offset angle of the principal axes of elasticity (θ) as

$$K = R(\theta) \begin{bmatrix} \omega_{0x}^2 & 0 \\ 0 & \omega_{0y}^2 \end{bmatrix} R'(\theta), \tag{13}$$

where R is a rotation matrix. In the open-loop rate mode, Automatic Gain Controller (AGC) and Phase Lock Loop (PLL) controllers are used to prevent variations in the vibration amplitude and the phase along the drive axis. Nevertheless, the coupling forces exerted along the drive axis can affect the resonant frequency of the drive axis. The method of sinusoidal phasor analysis was used to model the frequency changes in the drive axis. In our analysis, the phase of the vibration along the drive axis was used as the reference phase and, similar to the configuration of an open-loop CVG, a feedback force is used to control the amplitude of vibration along the drive axis in-phase with the velocity,

$$q(t) = \begin{bmatrix} x_a(t)e^{j\phi_x(t)} \\ (y_c(t) + jy_s(t))e^{j\phi_x(t)} \end{bmatrix}, F(t) = \begin{bmatrix} F_{xa}(t)je^{j\phi_x(t)} \\ 0 \end{bmatrix} \tag{14}$$

The first and second order time derivatives of position vector $(\dot{q}, \ddot{q})$ were calculated and substituted in Eqn. (11). The real and imaginary parts were separated and written in four equations. The steady-state equations (where $x_a(t) = X_a$, $\ddot{\phi_x} = 0$, $\dot{Y_s} = 0$, and $\dot{Y_c} = 0$) are:

$$\begin{aligned} -X_a\dot{\phi_x}^2 + 2\alpha\Omega\dot{\phi_x}Y_s + \omega_x^2 X_a + \omega_{xy}^2 Y_c = 0 \\ c_x X_a\dot{\phi_x} - 2\alpha\Omega\dot{\phi_x}Y_c + \omega_{xy}^2 Y_s = F_{xa}/m \\ -\dot{\phi_x}^2 Y_c - c_y\dot{\phi_x}Y_s + \omega_{xy}^2 X_a + \omega_y^2 Y_c = 0 \\ -\dot{\phi_x}^2 Y_s + c_y\dot{\phi_x}Y_c + 2\alpha\Omega X_a\dot{\phi_x} + \omega_y^2 Y_s = 0 \end{aligned} \tag{15}$$

These equations are a generic representation of the steady-state response of a CVG operating in the open-loop rate mode. The second equation can be used to estimate the magnitude of the AGC feedback force, but it is not needed for the SF analysis purposes. The remaining 3 nonlinear equations with 3 unknowns ($\dot{\phi_x}$, Y_c and Y_s) were numerically solved using MATLAB, estimating the vibration amplitude along the sense axis for different inputs of rotation (Ω). The phase of response along the sense axis in zero-rate input condition was used as a reference phase for decoupling the rate signal from the quadrature. The simulated SF and variations in the resonant frequency are shown in Fig. 4.

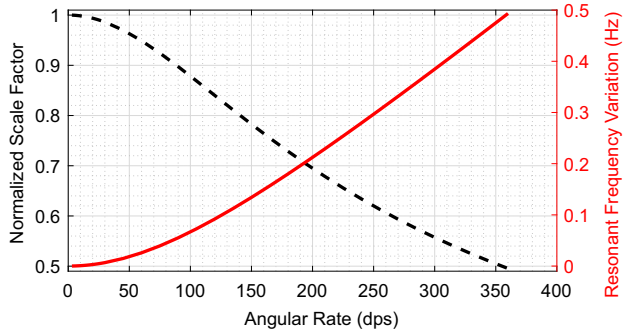

Fig. 4. Simulated data demonstrating the effect of modal coupling on the SF and the resonant frequency. The CVG parameters used for modeling are: $X_a = 0.1$, $\omega_{0x} = 15\ kHz$, $\Delta f = 0.5\ Hz$, $\theta = 10$ deg and $Q = 1M$.

From Eqn. (15), it is noted that variations in the resonant frequency of the drive axis, and consequently the SF, are dependent on the initial frequency split, quadrature, and quality factor. The modeling was repeated for different initial frequency splits and the results are shown in Fig. 5.

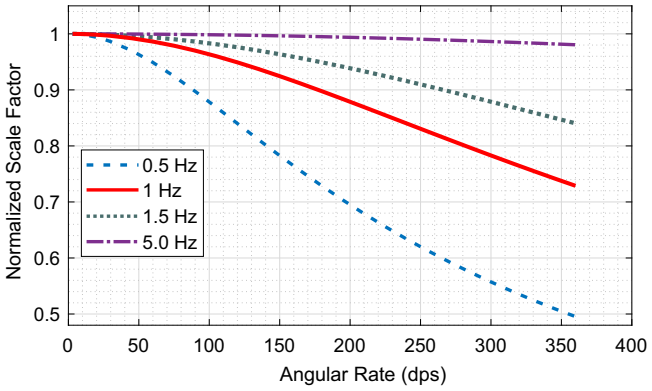

Fig. 5. Shown is the simulated SF of a CVG with fixed parameters of $X_a = 0.1$, $\omega_{0x} = 15\ kHz$, $\theta = 10$ deg, $\alpha = 0.8$, quality factor of 1M, and frequency splits varying from 0.5 Hz to 5 Hz.

IV. Nonlinear Capacitive Sensing

The third mechanism investigated in this paper is nonlinearity in parallel plate capacitive sensing. The output signal demodulated at the carrier frequency (ω_{car}) in the parallel plate sensing architecture with Electromechanical Amplitude Modulation (EAM) is approximated as,

$$V_s \approx \frac{1}{2} V_c R_G \frac{C_0}{g(1 - r sin(\omega_n t))^2}\dot{y}, \tag{16}$$

where V_c, R_G, C_0, g, ω_n, and r are the carrier voltage, transimpedance gain, sense capacitance, capacitive gap size, sense mode resonant frequency, and the normalized amplitude of vibration. Assuming a small enough normalized amplitude of vibration ($r = Y/g \approx 0$), the demodulated signal would

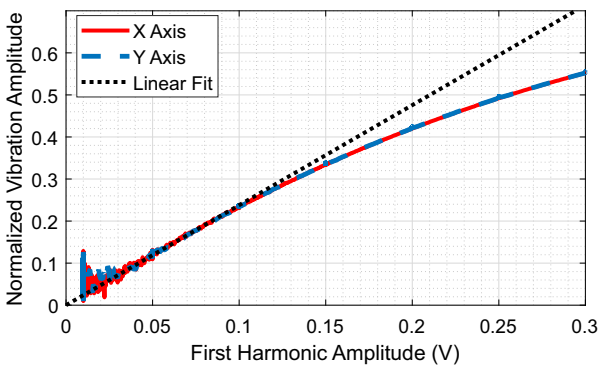

Fig. 6. Shown is the calculated normalized amplitude of vibration as a function of the demodulated amplitude of the first harmonic. Based on the design parameters, the capacitive gap size (g) is estimated to be 1.59 um.

give an accurate estimation of the velocity along the sense axis. However, the relation of the demodulated signal and the velocity is not linear for a large normalized amplitude of vibration and the signal would consist of an infinite number of harmonics with frequencies of $n\omega_n$ $(n = 1, 2, ...)$.

The linearity of the parallel plate capacitive sensing, using the first harmonic demodulation, can be characterized using the Side Band Ratio (SBR) method. In this method, the amplitude ratio of two consecutive order, or non-consecutive order, harmonics (i.e., the sidebands which are centered around the carrier frequency) can be used to estimate the normalized amplitude of vibration, [8]. Due to the differential detection scheme, a ratio of the first harmonic to the third harmonic was used to calculate the normalized amplitude of vibration,

$$R = \sqrt{V_{\omega_{car+3\omega_n}}/V_{\omega_{car+\omega_n}}}, \quad r = 2R/(R^2+1) \qquad (17)$$

For the DFP, the relation between the normalized amplitude of vibration and the amplitude of the first order harmonic is shown in Fig. 6. The results indicated that the accuracy of vibration amplitude estimation using the first order harmonics demodulation had an error less than 1% for output voltages below 100mV.

V. Experimental Results

In our experiment, a DFP with parameters shown in Fig. 1, was electrostatically tuned to a frequency split of 500mHz. The CVG was operated in the open-loop rate mode. The quadrature and the Coriolis signals were decoupled using I/Q synchronous demodulation. The SF was measured by rotating the sensor at constant angular rates up to 360 dps, Fig. 7. The experiment was repeated for different tuning voltages applied along the sense axis from 10V to 1V. The tuning voltage along the drive axis was regulated for each case to preserve the 0.5 Hz frequency split. By reducing the tuning voltage along the sense axis, a 27.7% reduction in the SF error was observed. The improvement in the linearity of the SF was explained by a reduced 3rd order nonlinearity in the CVG. The observed SF error at a low tuning voltage was determined to be converging to the SF error predicted by the modal coupling model.

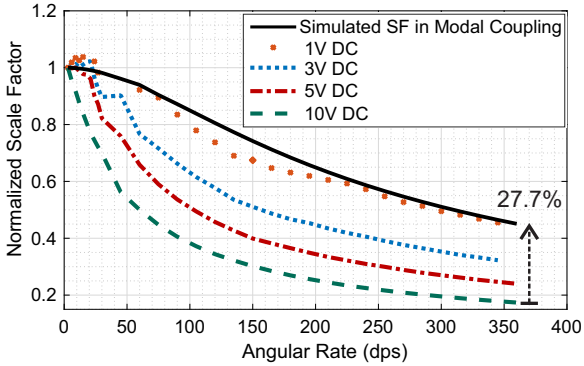

Fig. 7. Experimentally characterized SF for different tuning voltages acting along the sense axis. Simulated SF for a CVG with parameters of $\omega_x = 14.95\ kHz$, $\Delta f = 0.5\ Hz$, $\theta = 3.1\,\text{deg}$, $\alpha = 0.82$, $X_a = 0.140$ and quality factor of 1M using the mode coupled model explained in section 3.

In the experimental results, it was observed that the vibration amplitude along the sense axis did not exceed 100 mV for angular rotations up to 1 Hz. Therefore, it was concluded that nonlinearity in capacitive sensing was not contributing to the SF error in the 1 Hz dynamic range.

VI. Conclusion

In this paper, we identified the mechanisms which contribute to nonlinearity of SF in the open-loop angular rate mode of operation. The contribution of electro-mechanical nonlinearities, modal coupling, and nonlinear capacitive sensing was modeled and experimentally verified. Three conditions were determined to improve the linearity of SF in the angular rate mode of operation:

- Operation in a mode-mismatched condition improves the linearity of SF, though, degrades the sensitivity of the CVG.
- Mode-matching of CVG by removing the quadrature and frequency split and minimizing the electro-mechanical nonlinearities along the sense axis.
- Operation in the Force-to-Rebalanced (FRB) mode, which assures that no force will be exerted along the drive axis ($Y_s = 0$, $Y_c = 0$ in Eqn. (15)), results in a linear SF.

References

[1] D. Kim, et al., "Noise Analysis of Closed-Loop Vibratory Rate Gyros," American Control Conf. (ACC), Montreal, QC, Canada, Jun. 2012.
[2] S. Askari, et al., "Near-Navigation Grade Quad Mass Gyroscope with Q-factor Limited by Thermo-Elastic Damping," Solid-State Sensors, Actuators and MicroSystems Conf., Hilton Head, SC, USA, Jun. 2016.
[3] M. H. Asadian, et al., "High Quality Factor Mode Ordered Dual Foucault Pendulum Gyroscope," IEEE Sensors, New Delhi, India, Oct. 2018.
[4] M. H. Asadian, et al., "Characterization of Energy Dissipation Mechanisms in Dual Foucault Pendulum Gyroscopes," IEEE International Symposium on Inertial Sensors and Systems (INERTIAL), Naples, FL, USA, Apr. 2019.
[5] P. M. Polunin, et al., "Characterization of MEMS Resonator Nonlinearities Using the Ringdown Response," IEEE Journal of Microelectromechanical Systems, vol. 25, no. 2, pp. 297-303, 2016.
[6] N. N. Bogolyubov, et al., "Asymptotic Methods in the Theory of Non-Linear Oscillations", vol. 10. Boca Raton, FL, USA: CRC Press, 1961.
[7] A. S. Phani, et al., "Modal Coupling in Micromechanical Vibratory Rate Gyroscopes," IEEE Sensors Journal, vol. 6, no. 5, pp. 1144-1152, 2006.
[8] A. A. Trusov, et al., "A Novel Capacitive Detection Scheme with Inherent Self-Calibration," IEEE Journal of Microelectromechanical Systems, vol. 16, no. 6, pp. 1324-1333, 2007.